

X-RAY ABSORPTION, NUCLEAR INFRARED EMISSION AND DUST COVERING FACTORS OF AGN: TESTING UNIFICATION SCHEMES

S. MATEOS¹, F. J. CARRERA¹, A. ALONSO-HERRERO¹, A. HERNÁN-CABALLERO¹, X. BARCONS¹, A. ASENSIO RAMOS^{2,3},
M. G. WATSON⁴, A. BLAIN⁴, A. CACCIANIGA⁵, L. BALLO⁵, V. BRAITO⁶, C. RAMOS ALMEIDA^{2,3}

Draft version January 25, 2016

Abstract

We present the distributions of geometrical covering factors of active galactic nuclei (AGNs) dusty tori (f_2) using an X-ray selected complete sample of 227 AGN drawn from the Bright Ultra-hard *XMM-Newton* Survey. The AGN have z from 0.05 to 1.7, 2-10 keV luminosities between 10^{42} and 10^{46} erg s⁻¹ and Compton-thin X-ray absorption. Employing data from UKIDSS, 2MASS and the Wide-field Infrared Survey Explorer in a previous work we determined the rest-frame 1-20 μ m continuum emission from the torus which we model here with the clumpy torus models of Nenkova et al. Optically classified type 1 and type 2 AGN are intrinsically different, with type 2 AGN having on average tori with higher f_2 than type 1 AGN. Nevertheless, ~ 20 per cent of type 1 AGN have tori with large covering factors while ~ 23 -28 per cent of type 2 AGN have tori with small covering factors. Low f_2 are preferred at high AGN luminosities, as postulated by simple receding torus models, although for type 2 AGN the effect is certainly small. f_2 increases with the X-ray column density, which implies that dust extinction and X-ray absorption takes place in material that shares an overall geometry and most likely belongs to the same structure, the putative torus. Based on our results, the viewing angle, AGN luminosity and also f_2 determine the optical appearance of an AGN and control the shape of the rest-frame ~ 1 -20 μ m nuclear continuum emission. Thus, the torus geometrical covering factor is a key ingredient of unification schemes.

Keywords: galaxies: active - galaxies: nuclei - quasars: general - infrared: galaxies

1. INTRODUCTION

The simplest standard unified models postulate that the diversity of observed properties of active galactic nuclei (AGNs) can be largely explained as a viewing angle effect and anisotropic nuclear obscuration (Antonucci 1993; Urry & Padovani 1995). A key ingredient of these orientation-based models is an optically- and geometrically-thick toroidal structure located on tens of parsec scales that obscures the AGN nuclear region (accretion disk and X-ray corona) and the broad line region from certain lines-of-sight. For the sake of simplicity we will refer to this structure as the ‘torus’. Orientation-based unified models of tori with homogeneous dust distributions propose that AGN are optically classified as type 1 if they are observed at low inclinations with respect to the axis of the torus. In this case the line of sight does not intercept the material in the torus and we have an unobscured view of the central engine. On the other hand, AGN are optically classified as type 2 if they are observed at high inclinations where the material in the torus does intercept the line of sight obscuring the central engine (see Netzer 2015 for a recent review).

In recent years it has been realized that the AGN luminosity had to be incorporated as a key ingredient of unified models to explain the observed decrease in the relative fraction of type 2 objects at high AGN luminosities. Such a trend, mainly detected in X-ray surveys, has been further confirmed by surveys at optical and infrared wavelengths (e.g. Hasinger, Miyaji, & Schmidt 2005; Simpson 2005; Della Ceca et al. 2008; Treister, Krolik, & Dullemond 2008; Ebrero et al. 2009; Burlon et al. 2011; Ueda et al. 2014; Buchner et al. 2015; Assef et al. 2015; Lacy et al. 2015). To explain the scarcity of luminous type 2 AGN the ‘receding torus model’ has been often invoked. This model postulates that the luminosity-dependence of the type 2 AGN fraction is directly associated with the geometry of the torus in the sense that the covering factor of the torus (the fraction of the sky as seen by the source obscured by dust) decreases with increasing AGN luminosity (Lawrence 1991). Unfortunately, it is yet not fully understood how the AGN accretion power can influence the physical extent of the torus as there is substantial quantitative disagreement between published luminosity trends (e.g. Lawrence & Elvis 2010; Sazonov, Churazov, & Krivonos 2015).

The nuclear spectral energy distributions (SEDs) and mid-infrared interferometric observations of nearby AGN are modelled better with clumpy dusty tori, i.e. the obscuring material is not uniformly distributed inside the torus. In fact the material appears to be distributed in discrete, optically thick clumps (e.g. Alonso-Herrero et al. 2003; Tristram et al. 2007, 2009; Markowitz, Krumpe, & Nikutta 2014). X-ray spectral variability studies have also confirmed that the gas re-

¹ Instituto de Física de Cantabria (CSIC-Universidad de Cantabria), 39005, Santander, Spain; E-mail: mateos@ifca.unican.es

² Instituto de Astrofísica de Canarias, 38205, La Laguna, Tenerife, Spain

³ Departamento de Astrofísica, Universidad de La Laguna, 38206, La Laguna, Tenerife, Spain

⁴ Physics and Astronomy, University of Leicester, University Road, Leicester LE1 7RH, UK

⁵ INAF-Osservatorio Astronomico di Brera, via Brera 28, I-20121 Milano, Italy

⁶ INAF-Osservatorio Astronomico di Brera, Via Bianchi 46, I-23807 Merate (LC), Italy

sponsible for most of the X-ray absorption must be clumpy (e.g. Risaliti et al. 2009, 2011; Brenneman et al. 2013).

The clumpy nature of the dusty torus has very important implications for unification models as the classification of an AGN turns out to be an orientation-dependent probability. This means that even if we observe from an AGN’s equator there is some probability of classifying it as type 1, while a pole-on AGN could still be classified as type 2 if a single cloud intercepts the line of sight. Thus, while in the simplest orientation-based models with a smooth torus type 1 and type 2 AGN should have on average tori sharing the same properties, in the framework of ‘Clumpy Unification’ type 2 AGN should have tori with geometrical covering factors higher, on average, than type 1 AGN (for a recent review on this topic see Elitzur 2012). Recent analyses of the nuclear infrared emission of AGN with radiative transfer models of clumpy tori indicate that this might be indeed the case (Ramos Almeida et al. 2011; Ichikawa et al. 2015). Unfortunately until very recently such studies have been restricted to small samples of mostly nearby Seyfert galaxies and quasars (Mor, Netzer, & Elitzur 2009; Nikutta, Elitzur, & Lacy 2009; Ramos Almeida et al. 2009, 2011; Alonso-Herrero et al. 2011; Deo et al. 2011; Lira et al. 2013).

Thanks to the advent of the all-sky infrared survey conducted with the Wide Field Infrared Survey Explorer at 3.4, 4.6, 12 and 22 μm (*WISE*; Wright et al. 2010) it is now possible to constrain the properties of the AGN tori, in particular its geometrical covering factor, in large, representative samples of objects spanning a broad range of both redshifts and AGN luminosities.

The aim of this study is to verify observationally the validity of unified schemes in the framework of clumpy torus models. To do so we have determined, for the first time, the distribution of covering factors of AGN tori using a large, uniformly selected, complete sample of AGN. We have investigated whether type 1 and type 2 AGN are indeed intrinsically different objects, as recently claimed in the literature, by comparing the distributions of covering factors of their tori. Finally we have determined the dependence (or lack of) of the torus covering factor on the line of sight absorption measured in X-rays and the AGN luminosity.

The 227 AGN used in this study are drawn from the Bright Ultra-hard *XMM-Newton* Survey (BUXS; Mateos et al. 2012, 2015; hereafter M15). The objects have z in the range 0.05–1.7, intrinsic (absorption-corrected) 2–10 keV X-ray luminosities between 10^{42} and 10^{46} erg s^{-1} and X-ray absorption in the Compton-thin regime. There are a number of reasons why we have chosen the BUXS survey to conduct this study. Firstly, its large sample size and high spectroscopic identification completeness: BUXS is one of the largest (255 objects) complete flux-limited samples of bright AGN selected at energies above 4.5 keV with the *XMM-Newton* observatory. At the time of writing optical spectroscopic classifications and accurate redshifts are available for 98.4 per cent of the objects. Secondly, the rich set of multiwavelength data available for all sources: good quality *XMM-Newton* spectroscopy is available for the full sample, enabling accurate measurements of both the X-

ray absorption and intrinsic X-ray luminosities for all objects. Furthermore, 227 out of 233 AGN with X-ray luminosities and redshifts in the chosen intervals have rest-frame 1–20 μm nuclear photometric SEDs associated with the emission from the AGN dusty torus from M15. Clearly, all these properties make our AGN sample ideally suited to draw robust statistical constraints on the properties of the dusty torus of AGN.

From all the radiative transfer codes available in the literature to model the infrared emission associated with clumpy tori (e.g. Dullemond & van Bemmelen 2005; Nenkova, Ivezić, & Elitzur 2002, 2008a, 2008b henceforth referred to collectively as N08; Schartmann et al. 2008; Hönig et al. 2010; Stalevski et al. 2012; Siebenmorgen, Heymann, & Efstathiou 2015) we have chosen the N08 models, referred to as CLUMPY models, as they provide a good representation of the torus SED, and facilitate direct comparison with previous results in the literature (Mor, Netzer, & Elitzur 2009; Nikutta, Elitzur, & Lacy 2009; Alonso-Herrero et al. 2011; Deo et al. 2011; Ramos Almeida et al. 2009, 2011; Lira et al. 2013).

This paper is structured as follows. Section 2 describes the AGN sample used in this study. In Sections 3.1 and 3.2 we present the SED fitting techniques used to first isolate the emission associated with the torus and then to model it with the N08 models. In Section 3.3 we discuss our approach to determine the distributions of covering factors of AGN tori. In Section 4 our results are presented and discussed while in Section 5 we summarize our main results. Throughout this paper, errors are 68 per cent confidence for a single parameter, and we assume $\Omega_M=0.3$, $\Omega_\Lambda=0.7$ and $H_0=70$ $\text{km s}^{-1} \text{Mpc}^{-1}$.

2. AGN SAMPLE

The AGN in this study are drawn from the wide-angle Bright Ultra-hard *XMM-Newton* Survey (BUXS). BUXS is a complete flux-limited sample of 255 X-ray bright AGN ($f_{4.5-10 \text{ keV}} > 6 \times 10^{-14} \text{ erg s}^{-1} \text{ cm}^{-2}$) detected at 4.5 to 10 keV energies with the *XMM-Newton* European Photon Imaging Camera (EPIC)-pn (Strüder et al. 2001). The objects were selected at such high energies to reduce as much as possible biases against highly absorbed AGN. The survey covers 44.43 deg^2 of the northern sky (galactic latitudes $|b| > 20$ deg) distributed over 381 *XMM-Newton* observations having good quality for serendipitous source detection (Mateos et al. 2008, 2012). For full details on the survey design, sample selection and UV/optical spectroscopic identification and classification of the objects see Mateos et al. (2012, 2015). At the time of writing the identification completeness is 98.4 per cent (251 objects). Such a high identification rate guarantees that our study will not suffer from biases associated with optical identification incompleteness, that are more severe for highly obscured type 2 AGN.

We have good-quality *XMM-Newton* spectra for all BUXS sources, which constrain directly both the line of sight rest-frame absorbing column densities and X-ray luminosities (see M15). Throughout this paper L_X represents intrinsic, absorption corrected luminosities in the rest-frame 2–10 keV band.

For the analysis presented here we selected the 233 non-blazar AGN with $L_X > 10^{42}$ and $z < 1.7$. The luminosity cut was applied to reduce to a minimum the un-

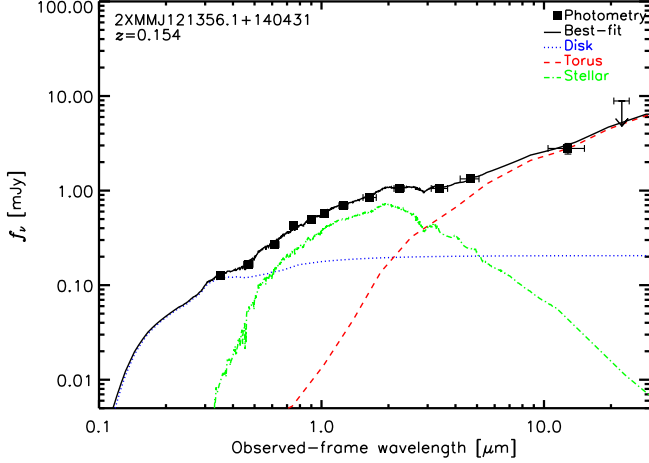


Figure 1. Example of the SED decomposition analysis used in M15 to isolate the AGN dusty torus emission (see Sec. 3.1 for details). The example corresponds to an AGN optically classified as type 1. Filled squares are the catalogued photometry. The dotted, dashed and dotted-dashed lines correspond to the accretion disk, torus (Seyfert 1 template from Silva, Maiolino, & Granato (2004)) and host galaxy emission, respectively. The solid line is the best-fit model. We note that in the SED decomposition analysis we treated all $22\mu\text{m}$ detections (168 in total) as upper limits (see M15 for details).

certainties associated with the determination of the infrared emission of the tori of our objects by increasing the contrast of the AGN over the underlying emission from the AGN hosts (12 objects removed; see Sec. 3.1). The redshift cut was imposed to assure adequate wavelength sampling of the torus rest-frame continuum emission (six objects removed). Finally, we excluded five type 1 AGN and one type 2 AGN without detections with signal-to-noise-ratio (SNR) > 2 at all 3.4 , 4.6 and $12\mu\text{m}$ in the final data release of *WISE* (AllWISE; Cutri et al. 2013). As the number of objects not detected with *WISE* above our selection threshold is rather small and, in addition, these objects span a broad range of L_X and z , removing them from the sample should not bias our results. All the above selection criteria left us with a sample of 227 AGN with L_X from 10^{42} to 10^{46}erg s^{-1} and $0.05 < z < 1.7$.

We classified our AGN as type 1 if permitted and semi-forbidden broad emission lines (line velocity widths $\gtrsim 1500\text{ km s}^{-1}$) were detected in their rest-frame UV/optical spectra (132 objects) and as type 2 if they showed narrow emission lines only (line velocity widths $< 1500\text{ km s}^{-1}$; 75 objects) or had a galaxy-like spectrum with no emission lines (3 objects). Due to the controversy regarding the nature of intermediate Seyfert types 1.8 and 1.9 as type 1 or type 2 AGN we kept such objects as a separate class (17 objects)⁷.

3. METHODOLOGY

3.1. Isolating the torus emission

In M15 we determined infrared SEDs associated with the emission from the dusty torus for the AGN in BUXS. To do so we conducted a thorough analysis of the rest-frame UV-to-infrared photometric SEDs to cor-

rect the catalogued infrared fluxes for any contamination associated with both the host galaxies and the direct emission from the AGN accretion disk. Our SEDs are based on data from the Sloan Digital Sky Survey (SDSS; Abazajian et al. 2009), the Two Micron All Sky Survey (2MASS; Jarrett et al. 2000; Cutri et al. 2013), the UKIRT Infrared Deep Sky Survey (UKIDSS; Lawrence et al. 2007) and WISE (Wright et al. 2010). To decompose the observed fluxes into AGN and galaxy emission we used the SED fitting tool SED Analysis using Bayesian Statistics (SEABAS⁸, Rovilos et al. 2014).

Very briefly, to model the emission from the accretion disk we used the type 1 quasar SED from Richards et al. (2006) at rest-frame wavelengths $\lambda < 0.7\mu\text{m}$ and a power-law $\lambda f_\lambda \propto \lambda^{-1}$ at longer wavelengths. To redden the accretion disk we used the Gordon & Clayton (1998) Small Magellanic Cloud extinction law at $\lambda < 0.33\mu\text{m}$ and the Cardelli, Clayton, & Mathis (1989) Galactic extinction law at $\lambda > 0.33\mu\text{m}$. In both cases we assumed $R_V = 3.1$. To characterize the continuum emission from the AGN dusty torus we used the Seyfert 1 and the two Seyfert 2 templates corresponding to rest-frame X-ray absorbing column densities $N_H < 10^{24}\text{ cm}^{-2}$ from Silva, Maiolino, & Granato (2004). Finally, to reproduce the emission from the stellar population of the AGN hosts at rest-frame optical-near-infrared wavelengths we used a library of 75 stellar templates from Bruzual & Charlot (2003). The templates have solar metallicity and a Chabrier initial mass function (Chabrier 2003) and were generated using 10 exponentially decaying star formation histories with characteristic times $\tau = 0.1\text{--}30\text{ Gyr}$ and a model with constant star formation, and a set of ages in the range $0.1\text{--}13\text{ Gyr}$. To redden the stellar templates we used the Calzetti et al. (2000) dust extinction law. An example of the SED decomposition analysis is illustrated in Fig. 1. It is important to highlight that we have adopted the same templates and SED-decomposition procedure to isolate the AGN torus emission of all sample objects.

In M15 we demonstrated that stellar contamination of catalogued fluxes in the infrared regime at rest-frame wavelengths shorter than $\sim 6\mu\text{m}$ is significant, especially for type 2 objects. Only for type 1 objects with $L_X > 10^{44}\text{ erg s}^{-1}$ the AGN outshines the host galaxy in the infrared band. The tight correlation found between rest-frame $6\mu\text{m}$ luminosities, corrected for contamination from the accretion disk and AGN hosts, and $2\text{--}10\text{ keV}$ intrinsic (absorption corrected) luminosities, supports the hypothesis that the infrared SEDs determined from our decomposition analysis are associated with dust heated by the intense radiation field of the AGN. This dust is most likely located in the putative torus on parsec scales. Hereafter, nuclear infrared SEDs will refer to the emission from the torus.

We focus our analysis here on rest-frame wavelengths longer than $1\mu\text{m}$ since this is the spectral region where the AGN torus emits the bulk of its radiation. Although in M15 we demonstrate that, at the luminosities of our AGN, contamination due to star formation at these wavelengths should be negligible, to minimize such effect we have treated the *WISE* $22\mu\text{m}$ fluxes of all 12 objects with $L_X < 5 \times 10^{42}\text{ erg s}^{-1}$ (five type 1 AGN,

⁷ Objects of intermediate Seyfert type 1.9 can be identified up to $z \sim 0.2\text{--}0.4$, depending on whether the $\text{H}\alpha$ emission line is outside the observable wavelength range of our spectroscopic data or not.

⁸ <http://astro.dur.ac.uk/~erovilos/SEABAS/>

Table 1

Parameters of the N08 CLUMPY torus models and range of values used in this work.

Parameter	Range
Torus angular width (σ)	[15°-70°]
Torus radial thickness (Y)	[5-30]
Mean number of clouds along equatorial rays (N_0)	[1-15]
Index of the radial distribution of clouds (q)	[0-3]
Single cloud optical depth (τ_V)	[5-150]
Viewing angle (i)	[0°-90°]

six type 2 AGN and one Sy1.9), whether detected or not at these wavelengths, as upper limits. Nevertheless, we have checked that this assumption does not affect our main results.

3.2. SED fitting with CLUMPY models

To describe the nuclear infrared emission of our objects we have used the radiative transfer models by N08. In these models the material obscuring the AGN nuclear region is treated as a medium with a toroidal shape where the dust and gas is distributed in high-density clumps inside it. The angular distribution of clouds has no sharp cutoff boundary and is described as a Gaussian of width σ ,

$$N_T(\beta) = N_0 e^{(-\beta^2/\sigma^2)} \quad (1)$$

where N_T is the line of sight number of clouds, $\beta = \pi/2 - i$ is the inclination angle of the torus equatorial plane with respect to the line of sight and i is the viewing angle from the torus axis. N_0 represents the mean number of clouds along radial equatorial rays. In the N08 models the radial distribution of clouds is parameterized as a power-law, $N(r) \propto r^{-q}$, where N is the number of clouds and q the power-law index. The torus radial thickness (Y) is defined as the ratio of the outer (R_o) to inner (R_d) radius of the distribution of clouds, where R_d is set by the AGN luminosity and the dust sublimation temperature (~ 1500 K in the model; Barvainis 1987). All clouds are assumed to be optically-thick and with the same optical depth, defined in the V band at 5500\AA . The model assumes a standard cold oxygen-rich interstellar medium (ISM) dust extinction law (Ossenkopf, Henning, & Mathis 1992). In addition to the parameters defining the geometry of the torus and the properties of the clouds, the scaling factor required to match the fluxes from the best-fit model to the observed values in the SEDs can be used as proxy for the AGN bolometric luminosity (see Nenkova et al. 2008b; Alonso-Herrero et al. 2011). We refer the reader to N08 for further details on CLUMPY models.

The online database of CLUMPY consists of more than 10^6 models based on a narrow grid for each torus parameter⁹. With such a fine grid we will not be able to distinguish between torus models based on different combinations of parameters but with differences in the continuum shape smaller than our SED photometric uncertainties. In that sense we can say that in our analysis there is a strong degeneracy in the parameters of CLUMPY models. To best deal with this issue we have conducted the SED fits using the code BayesCLUMPY from Asensio Ramos & Ramos Almeida (2009). This code has

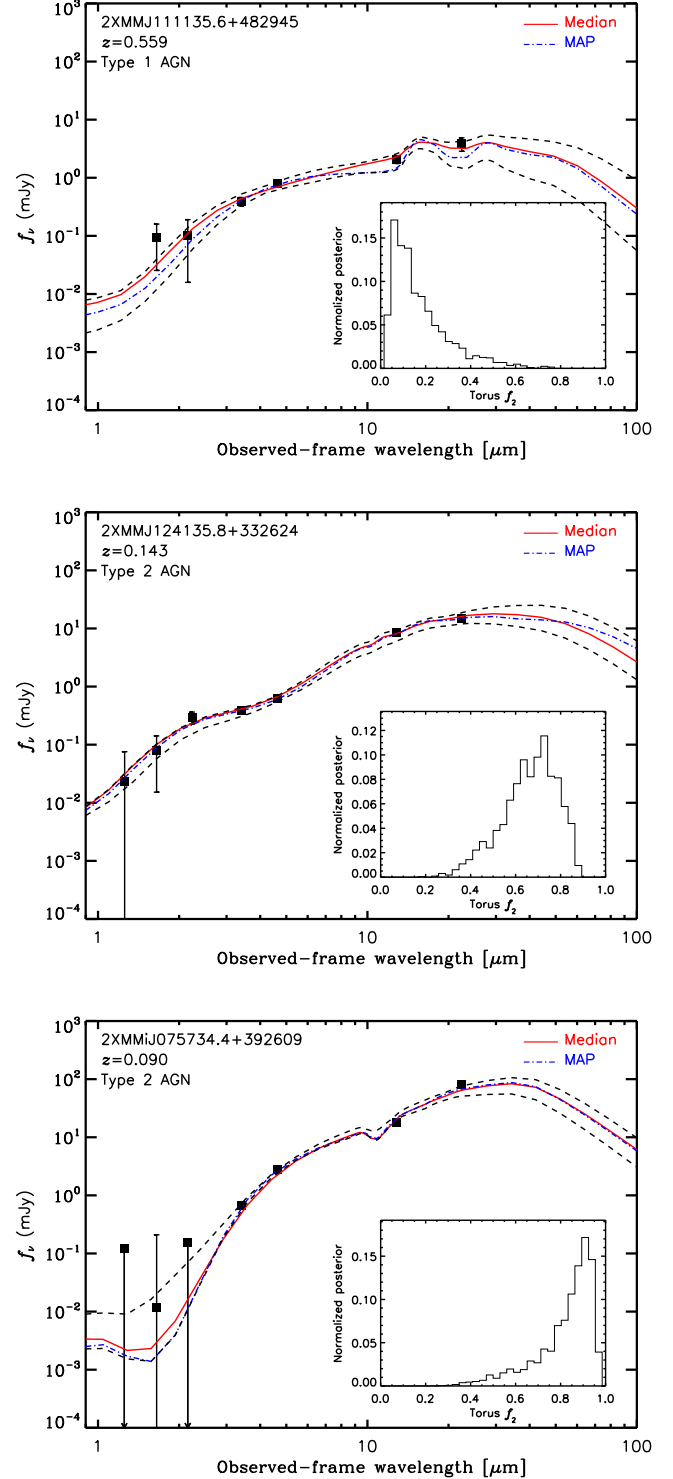


Figure 2. Examples of the SEDs of AGN dusty tori used in our study (filled symbols and error bars). Vertical arrows indicate upper limits. The SEDs have been corrected for the emission associated with both the accretion disk and the AGN host galaxies. The solid and dot-dashed lines correspond to the torus models described with the maximum (mode-MAP) and median values of the posterior probability distributions of the parameters returned by the BayesCLUMPY fits, respectively. The dashed lines indicate the range of models enclosing a 68 per cent probability. The inset plots show the normalized posterior distributions of f_2 from the fits.

⁹ <http://www.pa.uky.edu/clumpy/>

been especially developed to analyze the emission of AGN tori with CLUMPY models using a Bayesian inference approach. BayesCLUMPY uses a Metropolis-Hastings Markov Chain Monte Carlo (MCMC) sampling technique to determine posterior distributions for each parameter. To ensure the continuity of parameters, BayesCLUMPY also interpolates in the original database of models. In our analysis we have used truncated uniform prior distributions for all parameters in the ranges listed in Table 1.

3.3. Covering factors of AGN tori

In torus models with a clumpy distribution of dust the UV/optical appearance of an AGN depends on the viewing angle and the probability of intercepting a dusty cloud along our line of sight. Thus, the geometrical covering factor of the torus should play a fundamental role in the optical classification of AGN: the smaller the covering factor, the higher the probability of a direct view of the AGN nuclear region. Assuming that all individual clouds are optically thick, as in the N08 models, the probability that light from the AGN at an angle β will escape unaffected from the torus has the form

$$P_{\text{esc}}(\beta) = e^{-N_0 e^{(-\beta^2/\sigma^2)}} \quad (2)$$

The geometrical covering factor of the torus representing the fraction of the sky obscuring the AGN nuclear region, f_2 , is defined as

$$f_2 = 1 - \int_0^{\pi/2} P_{\text{esc}}(\beta) \cos(\beta) d\beta \quad (3)$$

where P_{esc} is integrated over all angles (Mor, Netzer, & Elitzur 2009). As f_2 is independent of the inclination angle, it represents the true intrinsic fraction of optically obscured type 2 objects in the entire AGN population.

Fig. 2 shows three examples of the typical nuclear infrared SEDs used in our study and the SED-fitting results obtained with BayesCLUMPY. The insets show the normalized posterior distributions of f_2 derived from the fits. To obtain the distribution of f_2 for a sample of objects fully taking into account the uncertainties from the fits we first concatenated together the individual arrays of values of f_2 returned from the MCMC analysis for each object and then we computed the probability distribution of the combined array of values of f_2 ¹⁰. To compare different distributions of f_2 we have used the two-sample Kolmogorov-Smirnov (KS) test and Monte Carlo simulations to determine the probability of rejecting the null hypothesis that the two samples are drawn from the same parent population. Each time we run our simulations we used bootstrap to randomly select 10^5 times the sample objects used to determine the distributions of f_2 .

For illustration purposes throughout this paper we have used a bin size of 0.03 to represent the distributions of f_2 but we stress that all computations are based

¹⁰ While we believe that the methodology applied is reliable, a more coherent way to infer the global distribution of the covering factor could have been to use a hierarchical Bayesian model. Nevertheless, such approach would have enjoyed the typical shrinkage of hierarchical modelling.

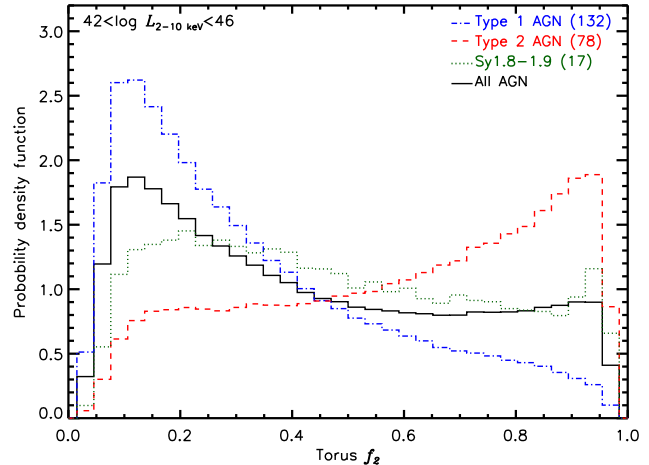


Figure 3. Distributions of the covering factors of AGN tori calculated for the full sample of objects.

on the arrays of values of f_2 . All distributions are normalized to have an area of one under the curve.

4. RESULTS

As indicated before, we have used the N08 models to reproduce the nuclear infrared emission associated with the dusty tori of AGN and to determine their dust covering factors. Therefore, the results inferred from our SED fits should be considered in the framework of these models.

4.1. f_2 versus optical class

Fig. 3 shows the distribution of f_2 for our full sample of AGN. It is evident that type 1 and type 2 AGN have significantly different distributions of f_2 , in the sense that type 2 AGN overall have tori with higher covering factors than type 1 AGN. Based on the KS test and our simulation analysis we can reject the null hypothesis that the two samples are drawn from the same parent population with a confidence level higher than 99.99 per cent. Nevertheless, we find that there is a large overlap between the distributions of f_2 for type 1 and type 2 AGN, in good agreement with previous studies based on high-spatial resolution nuclear infrared photometric data and/or mid-infrared spectroscopic data for small samples of local Seyferts and PG quasars (e.g. Mor, Netzer, & Elitzur 2009; Alonso-Herrero et al. 2011; Ramos Almeida et al. 2011, 2009; Ichikawa et al. 2015).

The distributions of f_2 that we find for the two AGN populations are significantly broader than claimed in the above studies. As we will see in the following sections such apparent discrepancies are not associated with higher uncertainties in our analysis compared to previous studies but to type 1 (type 2) AGN having rather large (small) torus covering factors. Since such objects are rare, sampling them requires studies of large and complete samples of AGN such as ours. For example, as we will see in Sec. 4.4.1, if we use $f_2=0.5$ as a threshold to separate AGN tori with low and high covering factors, we find that 26 out of 132 type 1 AGN have tori with high covering factors while 22 out of 78 type 2 AGN have tori with low covering factors.

As indicated before, we stress that we have used the

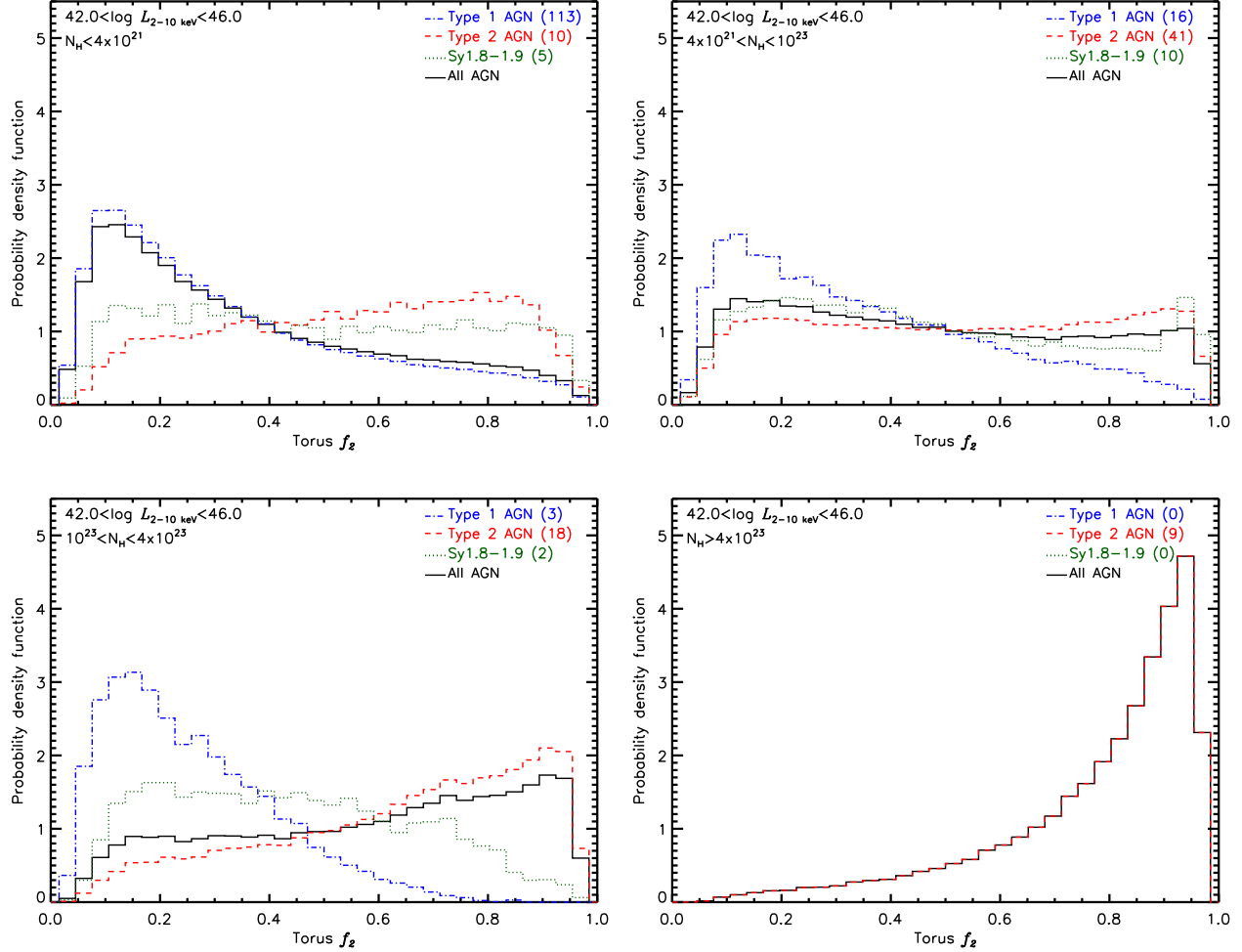


Figure 4. Dependence of the distribution of dust covering factors of AGN tori on the line of sight X-ray absorption.

same SED-decomposition procedure to isolate the AGN torus emission of all sample objects. Our SED fits with BayesCLUMPY take into account both the quality of the catalogued infrared photometric data, which is similar among our type 1 and type 2 AGN, and the uncertainties from the SED decomposition analysis. We have also checked that, the distributions of f_2 for type 1 AGN have widths, based on the 16th and 84th percentiles, indistinguishable from those of type 2 AGN. All this guarantees that any differences in the torus properties among AGN with different optical spectroscopic classifications reported here are genuine and not an artifact of either the SED decomposition analysis or the quality of the infrared data.

Interestingly, we find that AGN classified as Sy1.8-1.9 have a rather flat distribution of f_2 that is significantly different from those of type 1 and type 2 AGN. Thus from the infrared point of view, we find that it is highly unlikely that all Sy1.8-1.9 are simply ordinary type 1 AGN caught in a low flux state during the UV/optical spectroscopic observations, as significant differences exist between the properties of the tori of these two AGN classes. A KS test returns probabilities of 99.78 per cent and 97.98 per cent for rejecting the null hypothesis that the distributions of f_2 for Sy1.8-1.9 and those obtained for type 1 and type 2 AGN are identical. Therefore, al-

ternative processes must play a role. For example, our finding that 12 out of the 17 intermediate-type objects are absorbed in X-rays (see Sec. 4.2) favours a scenario where most of our Sy1.8-1.9 objects have broad-line regions reddened by optically-thin dust located either in the torus or on physical scales of the narrow-line region or the host galaxies (e.g. Alonso-Herrero et al. 2011).

We note that, if some high- z Sy1.8-1.9 objects are still present in our sample of type 2 AGN, the effect would be to reduce the differences between the f_2 distributions of type 1 and type 2 AGN. Clearly, this would not change our results since we have already found that we can reject the hypothesis that the distributions of f_2 for type 1 and type 2 AGN are drawn from the same parent population with a confidence level higher than 99.99 per cent.

Finally, we have used the results from our SED decomposition analysis to compare the distributions of f_2 for all objects with detected UV/optical broad emission lines (132 type 1 AGN and 17 Sy1.8-1.9s) with low and high extinction towards their accretion disk. To separate the objects we have used an extinction of $E(B-V)=0.32$, or $A_V \sim 1$ mag assuming a Galactic standard conversion. Such a value has often been used in the literature to identify moderately reddened type 1 AGN (e.g. Urrutia et al. 2012; Lacy et al. 2013 and references therein). Based on the chosen extinction threshold, 13 out of 132 type 1

AGN and 10 out of 17 Sy1.8-1.9s are classified as moderately reddened objects ($E(B-V)$ in the range 0.32-0.65; see M15 for details). We find that, as expected, higher f_2 are preferred in reddened broad-line AGN. According to the KS test we can reject the null hypothesis that the f_2 distributions of the two samples (reddened and unreddened broad-line AGN) are drawn from the same parent population with a 99.3 per cent confidence level.

Based on the results presented in this section we can conclude that, type 1, type 2 and probably also intermediate-type AGN, are on average intrinsically different, as has been reported previously in the literature (e.g. Ramos Almeida et al. 2011).

4.2. f_2 versus X-ray absorption

The discovery that the UV/optical spectroscopic classifications of AGN correlate well with the absorption properties measured in X-rays has lend strong observational evidence favouring standard orientation-based unified models. Nevertheless, it is well known that AGN exhibit a large range of dust-to-gas ratios and that, for a non-negligible fraction of objects, gas absorption in X-rays and dust extinction in the UV-to-infrared spectral band are not always detected together (e.g. Mainieri et al. 2002; Mateos et al. 2005a, 2005b; Tozzi et al. 2006; Garcet et al. 2007; Winter et al. 2009; Mateos et al. 2010; Corral 2011; Scott 2011; Page et al. 2011; González-Martín et al. 2014; Merloni et al. 2014).

To investigate whether a physical or geometrical connection exists between the material responsible for the X-ray absorption and UV-to-infrared obscuration, we have computed the distributions of f_2 for AGN with different levels of X-ray absorption. To have a good representation of both type 1 and type 2 AGN across the full range of measured X-ray column densities, we have divided the sample in four different bins: $N_H < 4 \times 10^{21} \text{ cm}^{-2}$ (henceforth X-ray unabsorbed), $4 \times 10^{21} < N_H < 10^{23} \text{ cm}^{-2}$, $10^{23} < N_H < 4 \times 10^{23} \text{ cm}^{-2}$ and $4 \times 10^{23} < N_H < 1.4 \times 10^{24} \text{ cm}^{-2}$. Fig. 4 summarizes the results of this analysis. Although in Fig. 4 we show the distributions of f_2 for objects classified as Sy1.8-1.9 for completeness, we do not use them in the analysis presented in this section as we are clearly limited by small number statistics. Nevertheless, our results suggest that the distribution of f_2 is rather flat for both X-ray unabsorbed and absorbed Sy1.8-1.9s.

We note that none of our X-ray selected sources has a best-fit X-ray column density in the Compton-thick regime. Nevertheless, considering the uncertainties in N_H , we cannot rule out unambiguously Compton-thick absorption in five type 2 AGN (all five sources belong to the $4 \times 10^{23} < N_H < 1.4 \times 10^{24} \text{ cm}^{-2}$ bin). As an independent test, we have determined the $L_X^{\text{obs}}/L_{6\mu\text{m}}$ luminosity ratio for these objects where, L_X^{obs} are observed (i.e. not corrected for intrinsic absorption) rest-frame 2-10 keV luminosities and $L_{6\mu\text{m}}$ are the monochromatic luminosities of the torus emission at rest-frame $6\mu\text{m}$. The later have been shown to be a good proxy for the AGN intrinsic power (Lutz et al. 2004; Ramos Almeida et al. 2007; Fiore et al. 2009; Georgantopoulos et al. 2011; Mateos et al. 2015; Stern 2015). Based on the relationship between L_X and $L_{6\mu\text{m}}$ from M15 we find that, in all five cases, the $L_X^{\text{obs}}/L_{6\mu\text{m}}$ ratio is consis-

tent with Compton-thin absorption. Finally, we have used a column density of $4 \times 10^{21} \text{ cm}^{-2}$ to separate unabsorbed and absorbed AGN. Assuming a Galactic standard dust-to-gas ratio, an N_H of $4 \times 10^{21} \text{ cm}^{-2}$ corresponds to $A_V \sim 2$ mag, or $E(B-V) \sim 0.65$, the extinction level that separates optical type 1 from type 2 AGN (Caccianiga et al. 2008; Merloni et al. 2014).

Interestingly we find that, type 1 and type 2 AGN with similar levels of X-ray absorption have significantly different distributions of torus geometrical covering factors. This result also holds for X-ray unabsorbed objects (Fig. 4 top left). We can reject the null hypothesis that the distributions of f_2 for X-ray unabsorbed type 1 and type 2 AGN are drawn from the same parent population with a confidence higher than 99.99 per cent. Clearly, intrinsic differences exist among the torus properties of these two groups of objects. Thus, although the host galaxies could totally outshine the AGN emission in the optical band in some objects (e.g. Moran, Filippenko, & Chornock 2002; Severgnini et al. 2003; Page et al. 2006), this cannot be the sole factor in determining the optical appearance of X-ray unabsorbed type 2 objects (Panessa & Bassani 2002, 2009; Bianchi et al. 2008, 2012; Gallo et al. 2013). Indeed only 4 out of 10 X-ray unabsorbed type 2 AGN in our sample have $L_X < 10^{43} \text{ erg s}^{-1}$, where host galaxy dilution can be an important effect (Caccianiga et al. 2007).

The distributions of f_2 for X-ray unabsorbed type 1 and type 2 AGN (Fig. 4 top left) are largely indistinguishable from those of absorbed AGN with N_H in the range $4 \times 10^{21} \text{ cm}^{-2} < N_H < 10^{23} \text{ cm}^{-2}$ (Fig. 4 top right). This suggests that up to column densities of $\sim 10^{23} \text{ cm}^{-2}$ there is no significant correlation between f_2 and N_H . Nevertheless, at $N_H < 10^{23} \text{ cm}^{-2}$ gas and dust in the AGN hosts might be contaminating some of our measurements, especially for type 2 AGN (e.g. Alonso-Herrero et al. 2003; Guainazzi, Matt, & Perola 2005; Goulding et al. 2012). Therefore we focus our attention on objects with column densities $N_H > 10^{23} \text{ cm}^{-2}$ as such high column densities should be associated with the torus¹¹. As we only have three type 1 objects with $N_H > 10^{23} \text{ cm}^{-2}$ in BUXS the distribution of f_2 for such objects may not be representative of the overall population of highly absorbed type 1 AGN. Thus, in what follows we restrict our discussion to type 2 objects. Nevertheless, we note that, based on the KS test and our simulation analysis, we cannot reject the null hypothesis that the distributions of f_2 for unabsorbed, mildly absorbed ($4 \times 10^{21} \text{ cm}^{-2} < N_H < 10^{23} \text{ cm}^{-2}$) and highly absorbed ($10^{23} \text{ cm}^{-2} < N_H < 4 \times 10^{23} \text{ cm}^{-2}$) type 1 AGN are drawn from the same parent population. We find that the covering factor of a typical type 2 AGN torus increases with N_H (Fig. 4 bottom plots). This effect becomes more pronounced at column densities approaching the Compton-thick regime.

Our analysis demonstrates that, not only AGN with different optical classifications have on average tori with different covering factors, but also that the most highly absorbed type 2 AGN have the highest covering factors

¹¹ Typical optical extinctions associated with galactic dust lanes are $A_V \sim 0.5-1.5$ mag. Such level of extinction corresponds to gas column densities of $N_H < 10^{23} \text{ cm}^{-2}$ for gas-to-dust ratios typical of nearby AGN (Maiolino et al. 2001). For example the column density towards the Galactic Center associated with molecular gas is $N_H \sim \text{a few } \times 10^{22} \text{ cm}^{-2}$ (Sanders, Solomon, & Scoville 1984).

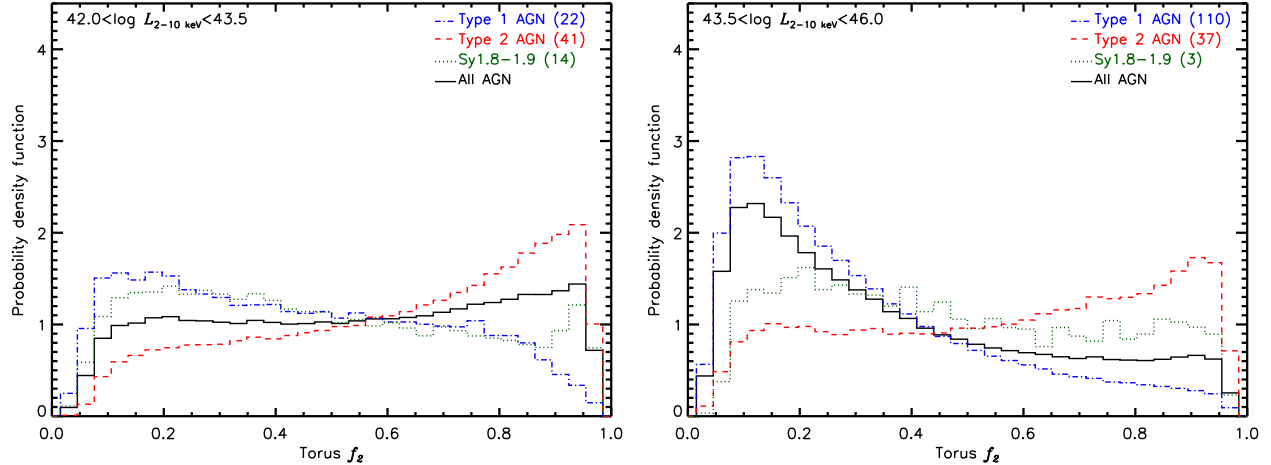


Figure 5. Dependence of the distribution of dust covering factors of AGN tori on the X-ray luminosity.

of nuclear dust. Since all sources with absorbing column densities $N_H > 4 \times 10^{23} \text{ cm}^{-2}$ have remarkably similar distributions of f_2 it is highly unlikely that statistical fluctuations associated with the small sample size affect our results. Such a high dust covering factors seem to be a common property of the most absorbed Compton-thin type 2 AGN (but see also Silva, Maiolino, & Granato 2004).

Interestingly, Ricci et al. (2011) found that, type 2 AGN with column densities in the range $10^{23} \text{ cm}^{-2} \leq N_H < 10^{24} \text{ cm}^{-2}$ have a stronger X-ray reflection component than both type 1 and type 2 AGN with $N_H < 10^{23} \text{ cm}^{-2}$. If the material in the torus is the main X-ray reflector, these results are consistent with a scenario where the covering factor of the torus is higher in the most highly absorbed Compton-thin type 2 AGN. This is supported by our findings.

X-ray spectral variability studies have shown that a large fraction of the X-ray absorbing cold gas must be located at the physical scales of the broad line region, probably in dust-free clouds in the innermost part of the torus, inside the dust sublimation radius (e.g. Elitzur 2008; Risaliti et al. 2009, 2011; Bianchi et al. 2012; Markowitz, Krumpe, & Nikutta 2014, and references therein). Our study supports these results, as the relationship between f_2 and N_H that we find implies that the dust and most of the X-ray absorbing gas are at least geometrically related and plausibly belong to the same structure, the putative torus.

4.3. f_2 versus AGN luminosity

Numerous works in the literature find that the relative fraction of type 2 AGN decreases with increasing AGN luminosity (e.g. Hasinger, Miyaji, & Schmidt 2005; Della Ceca et al. 2008; Treister, Krolik, & Dullemond 2008; Ebrero et al. 2009; Burlon et al. 2011; Ueda et al. 2014; Assef et al. 2015; Buchner et al. 2015; Lacy et al. 2015). These results have often been interpreted in the framework of the ‘receding torus’ model. According to this model the radius at which the dust sublimates increases with AGN luminosity, resulting in an increase of the opening angle of the torus and a decrease of its geometrical covering factor (Lawrence 1991). The end result is that the probability of finding an AGN as optical type 2 is lower at high AGN luminosities.

To investigate whether we find any evidence supporting a scenario where the AGN radiation field can affect the torus properties, we have determined the distributions of f_2 in two luminosity bins. The results are illustrated in Fig. 5. We clearly see that low covering factors are preferred in type 1s at high AGN luminosities. Although a similar trend is detected in type 2 objects, it is much less significant. This is somewhat expected as a decrease in the torus covering factor reduces the probability of identifying an AGN as optical type 2. We have compared the distributions of f_2 obtained at low and high AGN luminosities for the same class of objects using the KS test. We can reject the null hypothesis that the two samples are drawn from the same parent population only for type 1 AGN with a significance of 99.91 per cent.

Our sample of type 1 AGN reaches $z \sim 1.7$ while all type 2 AGN have $z \lesssim 1$. To avoid comparing objects at different evolutionary stages, we have also determined the distributions of f_2 in our two luminosity bins using type 1 and type 2 objects at $z < 1$. Our results do not change. We note that we reach the same conclusion adopting even lower redshift limits. This shows that, although the rest-frame infrared spectral regions sampled with our photometric data vary with the objects’ redshift, this has no effect on the f_2 distributions presented in Fig. 5. Therefore, we can conclude that our results are robust and they are consistent with a decrease of the covering factor of AGN tori with increasing AGN luminosity, although for X-ray selected type 2 AGN, the effect is modest. A detailed investigation of whether the detected changes of f_2 with luminosity are strong enough to explain the observed scarcity of type 2 AGN at high luminosities will be presented in a forthcoming paper.

4.4. Nuclear infrared continuum emission

4.4.1. Dependence on f_2

It is reasonable to expect that the properties of the nuclear infrared continuum emission of AGN, in particular the broad-band continuum shape, might depend directly on the covering factor of the torus. To investigate this issue we show in Fig. 6 (top plots) a compilation of all

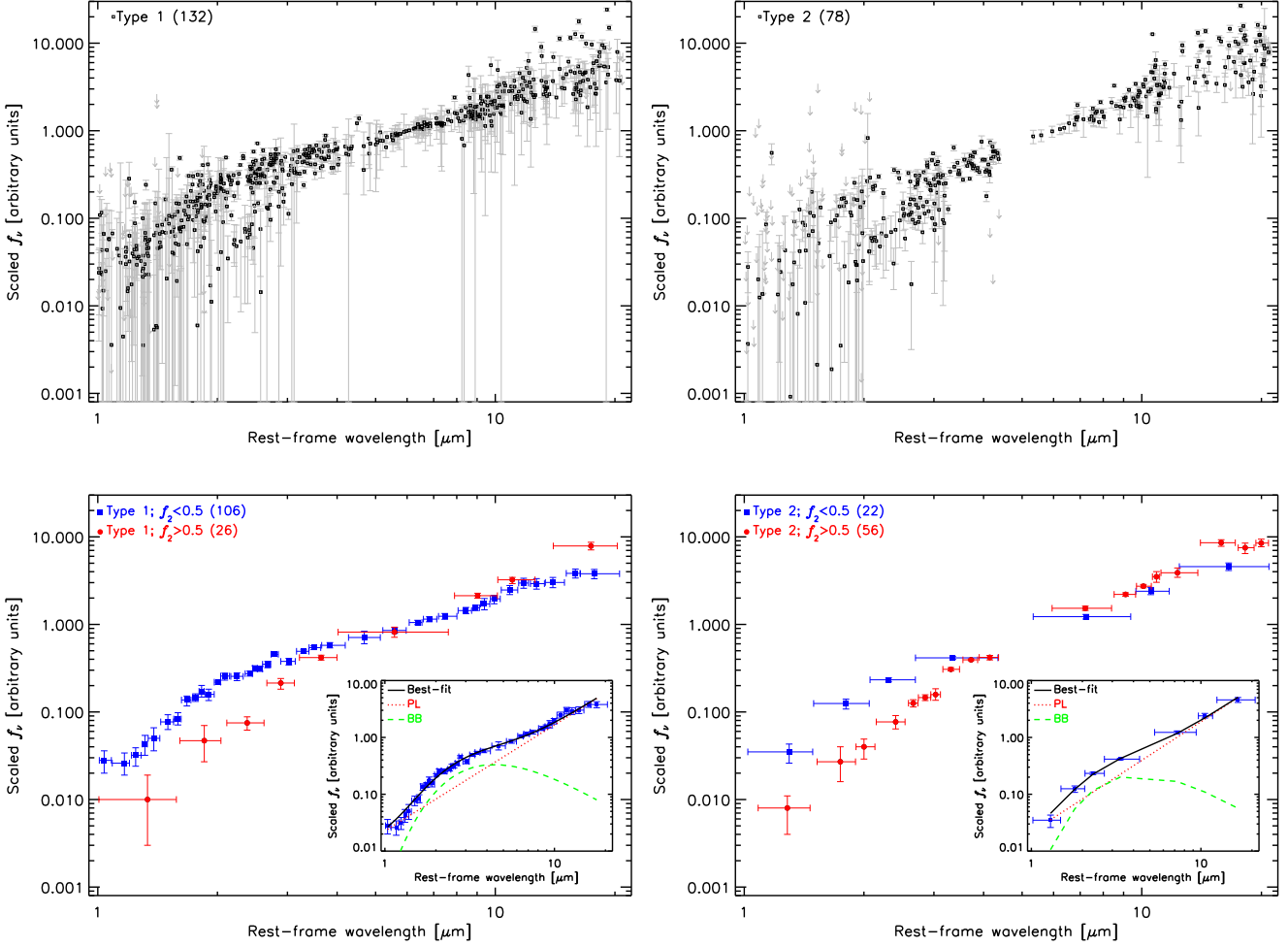


Figure 6. Top plots: nuclear torus-only infrared SEDs of our type 1 (left) and type 2 (right) AGN, respectively (small open symbols). Downward arrows represent upper limits. All SEDs are normalized at rest-frame $6\,\mu\text{m}$. Bottom plots: median SEDs of objects with low ($f_2 < 0.5$; large filled squares) and high ($f_2 > 0.5$; large filled circles) dust covering factors, respectively. The insets show the fits of the median SEDs of type 1 and type 2 objects with $f_2 < 0.5$ with a two-component phenomenological model consisting on a power-law (PL; dotted line) and a black-body (BB; dashed line). Solid lines represent the best-fit model (see Sec. 4.4.2 for details).

nuclear infrared SEDs of our AGN¹². As we are only interested in examining the continuum shape, we have normalized all SEDs at rest-frame $6\,\mu\text{m}$ to facilitate the comparison. To do so we have used linear interpolation in log-log space. We stress that we are only interested in the emission associated with the dusty torus, hence as indicated before, our nuclear infrared SEDs have been corrected for any contamination from the extrapolated accretion disk emission and, of course, the host galaxy.

The first result from Fig. 6 is that there is a large range of torus-only infrared continuum shapes for both type 1 and type 2 AGN. Clearly, at rest-frame wavelengths shorter than $\sim 20\,\mu\text{m}$ there is no canonical infrared slope for either AGN class (for similar results see also Alonso-Herrero et al. 2003; Lira et al. 2013). More importantly, we find that type 1 and type 2 AGN show a similar range of infrared continuum slopes although on

average type 2 AGN have steeper SEDs.

To investigate the role of the torus covering factor we have compared the SEDs of objects with tori with low ($f_2 < 0.5$) and high ($f_2 > 0.5$) covering factors, respectively. To assign the objects to the $f_2 < 0.5$ or $f_2 > 0.5$ class we have used the median values of the posterior distributions of f_2 obtained with the BayesCLUMPY SED fits for each source. We then moved all individual SEDs to rest-frame wavelengths and distributed the photometric data points into a common wavelength grid. The bins were defined to have at least 13 points and a minimum size of $0.01\,\mu\text{m}$. We have used the Astronomy Survival Analysis package (ASURV; Isobe, Feigelson, & Nelson 1986) to determine the median flux values in each bin taking into account both detections and upper-limits. To determine the errors of the median SEDs fully taking into account both the dispersion and errors in the individual fluxes we used Monte Carlo simulations. For each photometric point, if it was an upper-limit, we kept the values unchanged while for detections we generated random numbers using Gaussian distributions of mean and sigma, the flux measurements and their corresponding

¹² The upper limits indicate cases where, based on our SED decomposition analysis, the AGN accretion disk and host galaxy emission account for the full observed flux. In such cases the upper limit is the combined error of the fluxes associated with the accretion disk and host galaxy emission.

Table 2
Broad-band continuum shape of the observed and nuclear
infrared emission of AGN.

Class	f_2	N	$\langle L_X \rangle$	α_{torus}	$\alpha_{\text{torus}+\text{disk}}$	α_{obs}
(1)	(2)	(3)	(4)	(5)	(6)	(7)
Type 1	All	132	44.34	1.48 ± 0.06	1.34 ± 0.07	1.22 ± 0.07
Type 1	<0.5	106	44.41	1.40 ± 0.08	1.27 ± 0.08	1.14 ± 0.08
Type 1	>0.5	26	43.74	1.99 ± 0.13	1.70 ± 0.14	1.58 ± 0.11
Type 2	All	78	43.49	1.80 ± 0.07	1.74 ± 0.07	1.47 ± 0.08
Type 2	<0.5	22	43.95	1.61 ± 0.13	1.55 ± 0.14	1.23 ± 0.14
Type 2	>0.5	56	43.46	1.86 ± 0.08	1.81 ± 0.09	1.52 ± 0.10

Notes: (1): optical spectroscopic classification; (2): interval of torus geometrical covering factors of the sample; (3): number of objects; (4): median X-ray luminosity in logarithmic units; (5), (6) and (7): power-law indices of the median infrared continuum at rest-frame 5–20 μm in the following cases: the SEDs include only the emission associated with the torus (column 5); the SEDs include the emission associated with both the torus and the accretion disk (column 6); the SEDs include the emission associated with both the torus and the accretion disk and have not been corrected for any contamination associated with the host galaxies (column 7).

uncertainties, respectively. In cases where the simulated flux values were lower than zero, we replaced them with the corresponding flux uncertainties and treated them as upper-limits. We repeated the Monte Carlo exercise 10^4 times calculating each time median fluxes in the bins using the ASURV package, as we did for the real data. We then determined the uncertainties in our median SED fluxes using the 16th and 84th percentiles (68 per cent enclosed, equivalent to 1σ) of the distributions of simulated flux values on each bin. The results of this analysis are illustrated in Fig. 6 (bottom plots).

We clearly see that AGN with high f_2 have significantly redder SEDs on average than those with low f_2 . We find the same result for both type 1 and type 2 objects. As indicated in Table 2, type 1 (type 2) AGN with tori with low covering factors are on average about 5 (3) times more luminous than those with high covering factors. The observed differences in their nuclear infrared continuum emission could be a manifestation of the decrease of f_2 with AGN luminosity (see Sec. 4.3).

Interestingly, we find that ~ 20 per cent of type 1 AGN have tori with large, $f_2 > 0.5$, covering factors while ~ 28 per cent of type 2 AGN have tori with small, $f_2 < 0.5$, covering factors. As pointed out in Sec. 2, Seyfert 1.9 objects can only be identified up to $z \lesssim 0.4$ hence, some might still be present in our sample of type 2 AGN. To evaluate whether this has any impact on our results we have determined the fraction of type 2 AGN at $z < 0.3$ that have tori with $f_2 < 0.5$, finding a value of 22.7 per cent (10 out of 44 objects). We can safely conclude that ~ 23 –28 per cent of type 2 AGN have tori with small, $f_2 < 0.5$, covering factors.

To investigate whether differences exist in the continuum emission of AGN tori as a function of f_2 across the full range of wavelengths sampled, we have determined the spectral index that best describes the broad-band continuum emission of AGN tori at rest-frame 5–20 μm . We have used a phenomenological model consisting of a simple power-law¹³ which provides a good description of

¹³ We characterize the rest-frame 5–20 μm continuum as $f_\nu \propto \nu^{-\alpha}$, where α is the power-law index, ν are frequencies and f_ν are flux densities, respectively.

the data at these wavelengths. The results are shown in column 5 in Table 2. Although the numbers are broadly consistent, within the uncertainties, we find that type 2 AGN have on average steeper spectral indices than type 1 AGN. This is expected as, even within the chosen f_2 bins, the former AGN class has tori with higher covering factors overall than the later. Clearly, at rest-frame wavelengths longer than 5 μm differences still exist in the continuum emission of AGN tori, even among AGN of the same optical class.

Although, based on the shape of the torus continuum emission, type 1 and type 2 AGN are statistically different, there is no sharp division between the nuclear infrared SEDs of the two AGN populations. This implies that from the torus continuum emission alone, we cannot unambiguously distinguish type 1 and type 2 AGN.

Based on our results we can conclude that the covering factor of the torus is one of the main physical parameters controlling the shape of the nuclear infrared continuum emission of AGN. Significant differences exist in the properties of the torus emission, even among AGN of the same optical class, implying that infrared flux-limited population studies at rest-frame wavelengths shorter than ~ 5 –6 μm are not free of biases against the AGN with tori with the highest covering factors. We have shown in Sec. 4.2 that these objects are on average the most highly absorbed AGN in X-rays.

4.4.2. Near-infrared hot dust emission

A broad near-infrared bump above the extrapolation of the rest-frame $> 5 \mu\text{m}$ continuum is clearly detected in the SEDs of our type 1 and type 2 AGN with tori with low covering factors at rest-frame wavelengths ~ 1 –4 μm . The physical origin of such feature is still not clear. It could be associated with thermal radiation from hot dust in the innermost part of the torus heated by the AGN radiation field and with near sublimation temperatures (for graphite-type and silicate-type grains) or, alternatively, it might be emission from hot dust not associated with the torus (e.g. in the Narrow Line Region; Edelson & Malkan 1986; Barvainis 1987; Minezaki et al. 2004; Kishimoto et al. 2007; Schweitzer et al. 2008; Mor, Netzer, & Elitzur 2009; Riffel, Storchi-Bergmann, & McGregor 2009; Mor & Netzer 2012).

We have fitted the rest-frame 1–20 μm median SEDs of our type 1 and type 2 AGN with low torus covering factors with a two-component phenomenological model consisting of a power-law and a black-body to account for the near-infrared bump. We stress that this model is not physically motivated, nor are we claiming that the near-infrared bump originates in a separate component from the torus. Indeed, we find acceptable fits for all torus-only SEDs at rest-frame 1–20 μm with the N08 models and, after a careful visual check of the results from BayesCLUMPY, we find no evidence for additional components. The goal of our exercise is to compare the properties of the nuclear hot dust emission in type 1 and type 2 AGN. The results of the fits are illustrated in Fig. 6 (insets in the bottom plots).

The values obtained for the mean spectral indices of the mid-infrared broad-band continuum and black-body temperatures are $\alpha = 1.87 \pm 0.07$ and $T = 1154.2 \pm 33.2$ K for type 1 AGN and $\alpha = 1.95 \pm 0.12$ and $T = 1180.1 \pm 81.2$ K

for type 2 AGN. The best-fit temperatures indicate emission from very hot dust close to sublimation temperature. To determine the strength of the near-infrared bump we have computed its relative contribution to the integrated flux at rest-frame 2-7 μm . We found a contribution of 49.5 ± 3.4 per cent in type 1 AGN and $41.6^{+6.5}_{-7.8}$ per cent in type 2 AGN, respectively. Clearly, not only is the near-infrared bump not exclusively detected in type 1 AGN, but it also appears to have the same overall shape in type 1 and type 2 AGN with tori with low covering factors.

4.4.3. Contamination from the accretion disk and AGN hosts

So far, we have analysed nuclear infrared SEDs corrected for contamination from the extrapolated accretion disk emission and the AGN host galaxies. To compare our results with previous studies in the literature, which normally do not apply these corrections, we have analysed the median AGN SEDs that also include the emission from the accretion disk, and the median AGN SEDs based on the catalogued photometry, that include also the host galaxy emission. To do so we have followed the same approach as in Sec. 4.4.1, fitting the rest-frame 5-20 μm continuum emission with a simple power-law. The results are summarized in columns 6 and 7 in Table 2. Only when we used median SEDs based on catalogued fluxes did we obtain spectral indices consistent with the typical values reported in the literature, especially for type 1 AGN (e.g. Alonso-Herrero et al. 2006; Buchanan et al. 2006; Hernán-Caballero et al. 2009; Wu et al. 2009; Mullaney et al. 2011). This demonstrates that not only the emission from the accretion disk but also the stellar emission from the hosts can have a significant impact on the measured best-fit spectral indices of the infrared emission of AGN tori.

5. DISCUSSION AND CONCLUSIONS

Our study aims to test AGN unified models in the framework of clumpy torus models. To do so we have determined the distribution of dust covering factors of AGN tori using a large, uniformly selected, complete sample of 227 AGN. The AGN belong to the Bright Ultra-hard *XMM-Newton* Survey and have z in the range 0.05-1.7, and 2-10 keV intrinsic (absorption-corrected) luminosities between 10^{42} and 10^{46} erg s^{-1} .

Employing data from UKIDSS, 2MASS and WISE and a thorough SED decomposition analysis into AGN and galaxy emission, in a previous paper we determined the rest-frame 1-20 μm continuum emission associated with the torus for our sample objects. Here we modelled our nuclear infrared SEDs with the clumpy torus models of Nenkova et al. (2008a, 2008b) using the code BayesCLUMPY. This program has been especially developed to analyze the emission of AGN tori with the Nenkova et al. (2008a, 2008b) models using a Bayesian inference approach.

The main results of our analysis can be summarized as follows:

1. Type 1, type 2 and probably also intermediate-type AGN, are on average intrinsically different. Type 2 AGN have tori with higher geometrical covering

factors f_2 on average than type 1 AGN. Nevertheless, the distributions of f_2 for both type 1 and type 2 AGN are broad and there is a large overlap between the two populations. Although rare among all AGN, we find type 1 objects with large torus covering factors (26 out of 132) and type 2 objects with small torus covering factors (22 out of 78).

2. Interestingly, type 1 and type 2 AGN with similar levels of X-ray absorption have significantly different distributions of torus geometrical covering factors. This result also holds for X-ray unabsorbed type 1 and type 2 objects.
3. AGN classified as Sy1.8-1.9 have a rather flat distribution of f_2 that is significantly different from those of type 1 and type 2 AGN. Taking into account that most Sy1.8-1.9s are absorbed in X-rays (12 out of 17 objects) it is unlikely that all Sy1.8-1.9 are simply ordinary type 1 AGN caught in a low flux state during the UV/optical spectroscopic observations. Our results favour a scenario where most Sy1.8-1.9s have broad-line regions reddened by optically-thin dust located either in the torus or on physical scales of the narrow-line region or the host galaxies.
4. f_2 increases with the X-ray column density, at least at $N_{\text{H}} > 10^{23} \text{ cm}^{-2}$, which implies that dust extinction and X-ray absorption are geometrically related and plausibly belong to the same structure, the putative dusty torus.
5. Low f_2 values are preferred at high AGN luminosities, as postulated by simple receding torus models, although for X-ray selected type 2 AGN the effect is certainly small.
6. Based on our results, f_2 is one of the main physical parameters controlling the shape of the nuclear infrared emission of AGN. Although, from the shape of the torus continuum emission, type 1 and type 2 AGN are statistically different, there is no sharp division between the nuclear infrared SEDs of the two AGN populations. This implies that from the torus continuum emission alone, we cannot unambiguously distinguish type 1 and type 2 AGN.
7. A broad near-infrared bump at rest-frame $\sim 1\text{-}4 \mu\text{m}$ above the extrapolation of the rest-frame $> 5 \mu\text{m}$ infrared continuum is clearly detected in the SEDs of our type 1 and type 2 AGN having tori with low covering factors. We find that such spectral feature, which is often assumed to be due to hot dust in the inner-most part of the torus, is not exclusively detected in type 1 AGN and it has the same average properties in type 1 and type 2 AGN.

Based on the results presented here, all AGN are not intrinsically the same. This result applies not only to AGN with different optical classifications, but also to objects of the same optical class, in agreement with predictions from clumpy torus models. The AGN radiation field can modify the covering factor of the nuclear dust obscuring the central engine, although, at least in X-ray

selected type 2 objects, the effect is rather small. Furthermore, the covering factor of the torus increases with the X-ray column density, already for X-ray obscuration in the Compton-thin regime.

The reported significant differences in the torus emission, even among AGN of the same optical class, imply that infrared flux-limited population studies at rest-frame wavelengths shorter than $\sim 5\text{--}6\ \mu\text{m}$, are not free of biases against the most highly absorbed AGN, which we have shown are the objects with tori with the highest covering factors.

We can conclude that, the viewing angle, AGN luminosity and also f_2 determine the optical appearance of an AGN. Furthermore, f_2 controls the overall shape of the nuclear infrared continuum emission at rest-frame $\sim 1\text{--}20\ \mu\text{m}$. Thus, the geometrical covering factor of the dusty torus must be incorporated as a key ingredient of unification schemes.

We thank Nicolás Cardiel, R. Della Ceca and P. Severgnini for useful comments and discussions. This work is based on observations obtained with XMM-Newton, an ESA science mission with instruments and contributions directly funded by ESA Member States and NASA. Based on data from the Wide-field Infrared Survey Explorer, which is a joint project of the University of California, Los Angeles, and the Jet Propulsion Laboratory/California Institute of Technology, funded by the National Aeronautics and Space Administration. Funding for the SDSS and SDSS-II has been provided by the Alfred P. Sloan Foundation, the Participating Institutions, the National Science Foundation, the U.S. Department of Energy, the National Aeronautics and Space Administration, the Japanese Monbukagakusho, the Max Planck Society and the Higher Education Funding Council for England. The SDSS Web Site is <http://www.sdss.org/>. Based on observations collected at the European Organization for Astronomical Research in the Southern hemisphere, Chile, programme IDs 084.A-0828, 086.A-0612, 087.A-0447 and 088.A-0628. Based on observations made with the William Herschel Telescope and its service programme - operated by the Isaac Newton Group, the Telescopio Nazionale Galileo - operated by the Centro Galileo Galilei and the Gran Telescopio de Canarias installed in the Spanish Observatorio del Roque de los Muchachos of the Instituto de Astrofísica de Canarias, in the island of La Palma. SM, FJC, XB, A.H.-C. and A.A.-H. acknowledge financial support by the Spanish Ministry of Economy and Competitiveness through grant AYA2012-31447, which is partly funded by the FEDER programme. SM, FJC and A.A.-H. acknowledge financial support from the ARCHES project (7th Framework of the European Union, No. 313146). C.R.A. acknowledges financial support from the Marie Curie Intra European Fellowship within the 7th European Community Framework Programme (PIEF-GA-2012- 327934). AAR acknowledges financial support through the Ramón y Cajal fellowship and projects AYA2014-60476-P and Consolider-Ingenio 2010 CSD2009-00038 from the Spanish Ministry of Economy and Competitiveness. We thank the referee for the revision of the paper.

REFERENCES

- Abazajian K. N., et al., 2009, *ApJS*, 182, 543
 Alonso-Herrero A., Quillen A. C., Rieke G. H., Ivanov V. D., Efstathiou A., 2003, *AJ*, 126, 81
 Alonso-Herrero A., et al., 2006, *ApJ*, 640, 167
 Alonso-Herrero A., et al., 2011, *ApJ*, 736, 82
 Antonucci R., 1993, *ARA&A*, 31, 473
 Asensio Ramos A., Ramos Almeida C., 2009, *ApJ*, 696, 2075
 Assef R. J., et al., 2015, *ApJ*, 804, 27
 Barvainis R., 1987, *ApJ*, 320, 537
 Bianchi S., Corral A., Panessa F., Barcons X., Matt G., Bassani L., Carrera F. J., Jiménez-Bailón E., 2008, *MNRAS*, 385, 195
 Bianchi S., et al., 2012, *MNRAS*, 426, 3225
 Brenneman L. W., Risaliti G., Elvis M., Nardini E., 2013, *MNRAS*, 429, 2662
 Bruzual G., Charlot S., 2003, *MNRAS*, 344, 1000
 Buchanan C. L., Gallimore J. F., O’Dea C. P., Baum S. A., Axon D. J., Robinson A., Elitzur M., Elvis M., 2006, *AJ*, 132, 401
 Buchner J., et al., 2015, *ApJ*, 802, 89
 Burlon D., Ajello M., Greiner J., Comastri A., Merloni A., Gehrels N., 2011, *ApJ*, 728, 58
 Caccianiga A., Severgnini P., Della Ceca R., Maccacaro T., Carrera F. J., Page M. J., 2007, *A&A*, 470, 557
 Caccianiga A., et al., 2008, *A&A*, 477, 735
 Calzetti D., Armus L., Bohlin R. C., Kinney A. L., Koornneef J., Storchi-Bergmann T., 2000, *ApJ*, 533, 682
 Cardelli J. A., Clayton G. C., Mathis J. S., 1989, *ApJ*, 345, 245
 Corral, A., Della Ceca, R., Caccianiga, A., et al. 2011, *A&A*, 530, A42
 Cutri R. M., et al., 2013, Technical Report, Explanatory Supplement to the AllWISE Data Release Products
 Della Ceca R., et al., 2008, *A&A*, 487, 119
 Deo R. P., Richards G. T., Nikutta R., Elitzur M., Gallagher S. C., Ivezić Ž., Hines D., 2011, *ApJ*, 729, 108
 Chabrier G., 2003, *PASP*, 115, 763
 Dullemond C. P., van Bemmell I. M., 2005, *A&A*, 436, 47
 Ebrero J., et al., 2009, *A&A*, 493, 55
 Edelson R. A., Malkan M. A., 1986, *ApJ*, 308, 59
 Elitzur M., 2008, *NewAR*, 52, 274
 Elitzur M., 2012, *ApJ*, 747, L33
 Elitzur M., Ho L. C., Trump J. R., 2014, *MNRAS*, 438, 3340
 Fiore F., et al., 2009, *ApJ*, 693, 447
 Gallo L. C., MacMackin C., Vasudevan R., Cackett E. M., Fabian A. C., Panessa F., 2013, *MNRAS*, 433, 421
 Garcet O., et al., 2007, *A&A*, 474, 473
 Georgantopoulos I., et al., 2011, *A&A*, 534, A23
 González-Martín O., Díaz-González D., Acosta-Pulido J. A., Masegosa J., Papadakis I. E., Rodríguez-Espinoza J. M., Márquez I., Hernández-García L., 2014, *A&A*, 567, A92
 Gordon K. D., Clayton G. C., 1998, *ApJ*, 500, 816
 Goulding A. D., Alexander D. M., Bauer F. E., Forman W. R., Hickox R. C., Jones C., Mullaney J. R., Trichas M., 2012, *ApJ*, 755, 5
 Guainazzi M., Matt G., Perola G. C., 2005, *A&A*, 444, 119
 Hasinger G., Miyaji T., Schmidt M., 2005, *A&A*, 441, 417
 Hernán-Caballero A., et al., 2009, *MNRAS*, 395, 1695
 Hönig S. F., Kishimoto M., Gandhi P., Smette A., Asmus D., Duschl W., Polletta M., Weigelt G., 2010, *A&A*, 515, A23
 Ichikawa K., et al., 2015, *ApJ*, 803, 57
 Isobe T., Feigelson E. D., Nelson P. I., 1986, *ApJ*, 306, 490
 Jarrett T. H., Chester T., Cutri R., Schneider S., Skrutskie M., Huchra J. P., 2000, *AJ*, 119, 2498
 Kishimoto M., Hönig S. F., Beckert T., Weigelt G., 2007, *A&A*, 476, 713
 Lacy M., et al., 2013, *ApJS*, 208, 24
 Lacy M., Ridgway S. E., Sajina A., Petric A. O., Gates E. L., Urrutia T., Storrie-Lombardi L. J., 2015, *ApJ*, 802, 102
 Lawrence A., 1991, *MNRAS*, 252, 586
 Lawrence A., et al., 2007, *MNRAS*, 379, 1599
 Lawrence A., Elvis M., 2010, *ApJ*, 714, 561
 Lira P., Videla L., Wu Y., Alonso-Herrero A., Alexander D. M., Ward M., 2013, *ApJ*, 764, 159
 Lutz D., Maiolino R., Spoon H. W. W., Moorwood A. F. M., 2004, *A&A*, 418, 465
 Mainieri V., Bergeron J., Hasinger G., Lehmann I., Rosati P., Schmidt M., Szokoly G., Della Ceca R., 2002, *A&A*, 393, 425
 Maiolino R., Marconi A., Salvati M., Risaliti G., Severgnini P., Oliva E., La Franca F., Vanzì L., 2001, *A&A*, 365, 28

- Markowitz A. G., Krumpe M., Nikutta R., 2014, MNRAS, 439, 1403
- Mateos, S., Barcons, X., Carrera, F. J., et al. 2005a, A&A, 433, 855
- Mateos, S., Barcons, X., Carrera, F. J., et al. 2005b, A&A, 444, 79
- Mateos S., et al., 2008, A&A, 492, 51
- Mateos, S., Carrera, F. J., Page, M. J., et al. 2010, A&A, 510, A35
- Mateos S., et al., 2012, MNRAS, 426, 3271
- Mateos S., et al., 2015, MNRAS, 449, 1422
- Merloni A., et al., 2014, MNRAS, 437, 3550
- Minezaki T., Yoshii Y., Kobayashi Y., Enya K., Suganuma M., Tomita H., Aoki T., Peterson B. A., 2004, ApJ, 600, L35
- Hasinger G., Miyaji T., Schmidt M., 2005, A&A, 441, 417
- Mor R., Netzer H., Elitzur M., 2009, ApJ, 705, 298
- Mor R., Netzer H., 2012, MNRAS, 420, 526
- Moran E. C., Filippenko A. V., Chornock R., 2002, ApJ, 579, L71
- Mullaney J. R., Alexander D. M., Goulding A. D., Hickox R. C., 2011, MNRAS, 414, 1082
- Nenkova M., Ivezić Ž., Elitzur M., 2002, ApJ, 570, L9
- Nenkova M., Sirocky M. M., Nikutta R., Ivezić Ž., Elitzur M., 2008, ApJ, 685, 160
- Nenkova M., Sirocky M. M., Ivezić Ž., Elitzur M., 2008, ApJ, 685, 147
- Netzer H., 2015, ARA&A, 53, 365
- Nikutta R., Elitzur M., Lacy M., 2009, ApJ, 707, 1550
- Ossenkopf V., Henning T., Mathis J. S., 1992, A&A, 261, 567
- Panessa F., Bassani L., 2002, A&A, 394, 435
- Panessa F., et al., 2009, MNRAS, 398, 1951
- Page M. J., et al., 2006, MNRAS, 369, 156
- Page M. J., Carrera F. J., Stevens J. A., Ebrero J., Blustin A. J., 2011, MNRAS, 416, 2792
- Ramos Almeida C., Pérez García A. M., Acosta-Pulido J. A., Rodríguez Espinosa J. M., 2007, AJ, 134, 2006
- Ramos Almeida C., et al., 2009, ApJ, 702, 1127
- Ramos Almeida C., et al., 2011, ApJ, 731, 92
- Ricci C., Walter R., Courvoisier T. J.-L., Paltani S., 2011, A&A, 532, A102
- Richards G. T., et al., 2006, AJ, 131, 2766
- Riffel R. A., Storchi-Bergmann T., McGregor P. J., 2009, ApJ, 698, 1767
- Risaliti G., et al., 2009, MNRAS, 393, L1
- Risaliti G., Nardini E., Salvati M., Elvis M., Fabbiano G., Maiolino R., Pietrini P., Torricelli-Ciamponi G., 2011, MNRAS, 410, 1027
- Rovilos E., et al., 2014, MNRAS, 438, 494
- Sanders D. B., Solomon P. M., Scoville N. Z., 1984, ApJ, 276, 182
- Sazonov S., Churazov E., Krivonos R., 2015, MNRAS, 454, 1202
- Schartmann M., Meisenheimer K., Camenzind M., Wolf S., Tristram K. R. W., Henning T., 2008, A&A, 482, 67
- Severgnini P., et al., 2003, A&A, 406, 483
- Siebenmorgen R., Heymann F., Efstathiou A., 2015, arXiv, arXiv:1508.04343
- Silva L., Maiolino R., Granato G. L., 2004, MNRAS, 355, 973
- Simpson C., 2005, MNRAS, 360, 565
- Scott, A. E., Stewart, G. C., Mateos, S., et al. 2011, MNRAS, 417, 992
- Schweitzer M., et al., 2008, ApJ, 679, 101
- Stalevski M., Fritz J., Baes M., Nakos T., Popović L. Č., 2012, MNRAS, 420, 2756
- Stern D., 2015, ApJ, 807, 129
- Strüder L., et al., 2001, A&A, 365, L18
- Tozzi P., et al., 2006, A&A, 451, 457
- Treister E., Krolik J. H., Dullemond C., 2008, ApJ, 679, 140
- Tristram K. R. W., et al., 2007, A&A, 474, 837
- Tristram K. R. W., et al., 2009, A&A, 502, 67
- Ueda Y., Akiyama M., Hasinger G., Miyaji T., Watson M. G., 2014, ApJ, 786, 104
- Urrutia T., Lacy M., Spoon H., Glikman E., Petric A., Schulz B., 2012, ApJ, 757, 125
- Urry C. M., Padovani P., 1995, PASP, 107, 803
- Winter L. M., Mushotzky R. F., Reynolds C. S., Tueller J., 2009, ApJ, 690, 1322
- Wright E. L., et al., 2010, AJ, 140, 1868
- Wu Y., Charmandaris V., Huang J., Spinoglio L., Tommasin S., 2009, ApJ, 701, 658